Separation Shock Dynamics In Mach 5 Turbulent Interactions Induced by Cylinders

D. S. Dolling* and D. R. Smith†
University of Texas at Austin, Austin, Texas

Wall pressure fluctuations have been measured under the unsteady separation shock in interactions generated by unswept circular cylinders. Models were tested in the turbulent boundary layers on the tunnel floor and on a full-span flat plate. The nominal freestream Mach number was 5, the freestream unit Reynolds number $53 \times 10^6\ m^{-1}$, and the wall temperature approximately adiabatic. Using a conditional sampling algorithm, distributions of the shock frequency, shock period, and shock speeds in the upstream and downstream directions have been calculated. The shock frequency distributions are broadband, and the most probable frequencies are low, typically less than 2 kHz. The mean and maximum shock speeds are also low, about 6 and 20% of the freestream velocity, respectively. The results support a simple model suggesting that pressure fluctuations in the separated flow may drive the shock motion.

I. Introduction

SINCE the onset of supersonic flight, shock-induced turbulent boundary-layer separation has been of considerable interest to vehicle designers, since it occurs in such a wide variety of internal and external aerodynamics problems. Shock-induced separation is now known to be an unsteady phenomenon characterized by large-scale, low-frequency shock motion.[1] In this context, "low frequency" implies low relative to the typical eddy frequency U_e/δ_0 in the incoming boundary layer, where U_e and δ_0 are the edge velocity and velocity thickness, respectively. The meaning of "large-scale" is discussed in the example below.

A typical wall pressure signal upstream of S, the separation line deduced from surface tracers, in a Mach 3 compression ramp interaction is shown in Fig. 1a. The moving separation shock wave generates an intermittent wall pressure signal and a rapid rise in the standard deviation σ_{P_w} (Fig. 1b). The intermittency γ, shown in Fig. 1c, is the fraction of the time that the shock is upstream of a given station. The streamwise distance over which γ increases from 0 to 1 gives the length scale of the shock motion. In all of the cases known to the authors, the shock moves from X_0, which is where the mean wall pressure $\bar{P}_w$ first increases, to just upstream of S. Depending on flowfield type, this distance can vary from a fraction of δ_0 to several δ_0. The available evidence suggests that there is a single unsteady separation shock wave, not a streamwise rippling compression fan.[1]

A large fraction of the recent work in this area has been done at Mach 3 in the Princeton University blowdown tunnel using hemicylindrically blunted fins,[2] unswept compression ramps,[3-6] and sharp fins at angle of attack.[7-9] A reanalysis of the blunt fin data of Ref. 2 using a new conditional sampling algorithm was recently reported in Ref. 10. The results suggested that the separation shock zero-crossing frequency f_c (defined as the number of shock crossings per second at a given station) might be independent of the incoming boundary-layer properties and dependent only on the diameter D of the blunt fin. However, this was based on a sparse data set obtained at a low sampling frequency. Further, spatial resolution was poor such that $(f_c)_{max}$, the maximum value of f_c, was not well defined. In another recent study using circular cylinders at Mach 5, a similar dependence of f_c on D was observed, but the effects, if any, of boundary-layer properties could not be assessed since the tests were done at a single station on a flat plate.[11]

The purpose of the present study was to address this question. Experiments were conducted in the same Mach 5 tunnel as the work of Ref. 11 and at the same freestream conditions. The same circular cylinders were also used but were tested on the tunnel floor ($\delta_0 = 1.62$ cm) rather than on a flat plate ($\delta_0 = 0.54$ cm). Further, in Ref. 11 and in the present tests, high sampling rates were used and better spatial resolution was obtained than in the earlier Mach 3 study. The main objective of the study was to determine the effects of the incoming boundary-layer properties on the separation shock motion—in particular, the effects on the zero crossing fre-

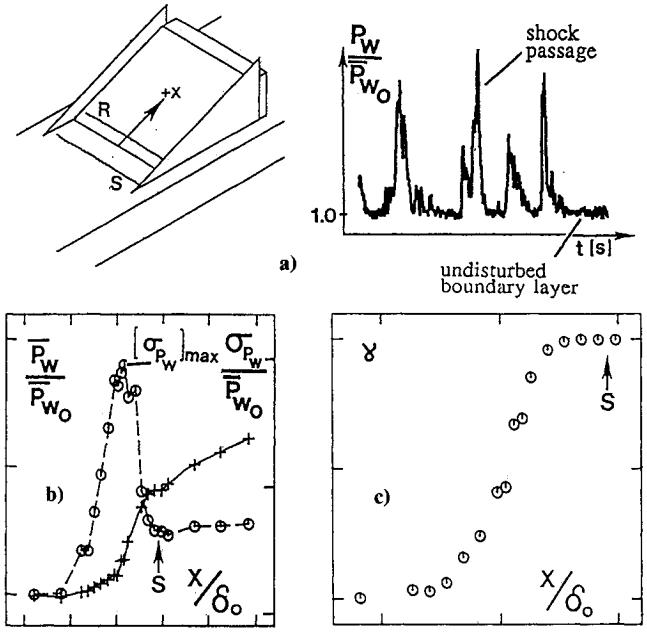

Fig. 1 Shock-induced separation: a) wall pressure signal; b) distributions of mean and standard deviation; c) intermittency.

Presented as Paper 88-0305 at the AIAA 26th Aerospace Sciences Meeting, Reno, NV, Jan. 11-14, 1988; received Feb. 22, 1988; revision received Dec. 20, 1988.

*Associate Professor, Department of Aerospace Engineering and Engineering Mechanics. Associate Fellow AIAA.

†Graduate Student, Department of Aerospace Engineering and Engineering Mechanics. Currently Captain, U.S. Air Force.

quency, shock period and frequency distributions, and shock speeds in the upstream and downstream directions.

II. Experimental Program

Test Facility and Models

The tests were conducted in the Mach 5 blowdown facility of the University of Texas at Austin. This facility has a 17.8 × 15.2 cm (7 × 6 in.) test section. The tests were conducted on the tunnel floor, close to the nozzle exit plane. The earlier work of Ref. 11 was done on a full-span flat plate, 43.7 cm (18 in.) long, at zero angle of attack. In both test series, two Kulite transducers were installed flush with the surface, or very slightly recessed, in a circular, rotatable plug upstream of an unswept circular cylinder (Fig. 2). Hanly[12] has shown that a slightly protruding transducer has a large effect on the rms pressure level and spectral content whereas a small recess has little effect. Two cylinders, with $D = 1.27$ and 1.91 cm (0.5 and 0.75 in.), were used in both studies. Their heights were 8.89 and 7.62 cm (3.5 and 3.0 in.), respectively, which, based on the criterion of Ref. 13, renders them effectively semi-infinite. The cylinder was moved relative to the fixed transducers. Over the range of travel, at maximum 2.5 cm (1 in.), the small changes in incoming flow conditions have a negligible effect on the interaction.

Instrumentation

Most tests in this study and in Ref. 11 were conducted using Kulite model XCW-062-15A transducers, spaced 0.29 cm (0.115 in.) apart center-to-center. Full-scale output is nominally 225 mV, giving a sensitivity of 2.2 mV/10^3 Nm^{-2} (15 mV/psi). The natural frequency of the transducer's silicon diaphragm is quoted by the manufacturer as 250 kHz. Some additional tests used model XCQ-062-50A transducers. These have a higher range (3.45×10^5 Nm^{-2}, 50 psi) and a lower sensitivity (0.22 mV/10^3 Nm^{-2}, 1.5 mV/psi) but a higher diaphragm natural frequency (500 kHz). Both transducer models have external diameters of 0.162 cm (0.062 in.) and diaphragm diameters of 0.071 cm (0.028 in.). Their combined nonlinearity and hysteresis are quoted as 0.5% full-scale. The transducers were calibrated statically daily. Shock tube tests using similar transducer designs have shown that dynamic and static calibrations differ by only a few percent.[14]

The output from the transducers was amplified by Measurements Group Inc. model 2300 amplifiers with gains of 100–2300, depending on location in the interaction. The signals were low-pass filtered using Ithaco model 4213 filters with the cutoff set either to one-half the sampling rate f_s or, for $f_s > 100$ kHz, at 50 kHz. This was because the dynamic response of the transducers was limited to about 50 kHz. The signal was digitized by a Masscomp 12 bit analog/digital (a/d) converter equipped with sample-and-hold, which outputs 0–4096 counts for inputs of 0–10 V. The overall signal-to-noise ratio was about 10 : 1 in the undisturbed boundary layer and about 100 : 1 in the intermittent region. Additional details are given in Refs. 11 and 15.

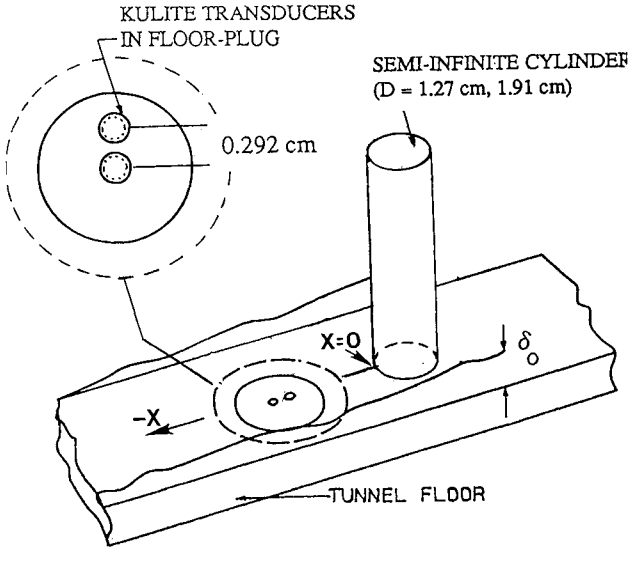

Fig. 2 Model and coordinate system.

Table 1 Incoming flow parameters

Parameter	Tunnel floor	Flat plate
M_∞	4.90 ± 0.02	4.96 ± 0.02
U_∞	741 m/s (2432 ft/s)	739 m/s (2424 ft/s)
Re_∞	53.3×10^6 m^{-1} (16.2×10^6 ft^{-1})	53.1×10^6 m^{-1} (16.2×10^6 ft^{-1})
T_0	330 K (595°R)	327 K (590°R)
P_0	2.09×10^6 N/m^2 (304 psi)	2.09×10^6 N/m^2 (303 psi)
δ_0	1.62×10^{-2} m (0.63 in.)	5.36×10^{-3} m (0.25 in.)
δ^*	5.23×10^{-3} m (0.206 in.)	2.18×10^{-3} m (0.086 in.)
θ	4.54×10^{-4} m (1.83×10^{-2} in.)	1.81×10^{-4} m (7.13×10^{-3} in.)
Π	0.115	0.47
Re_θ	23.4×10^3	8.99×10^3
C_f	9.9×10^{-4}	1.01×10^{-3}

Flow Conditions

The freestream and incoming turbulent boundary-layer properties expressed using standard terminology for both test series are given in Table 1. They are discussed further in Sec. IV. In both cases, the boundary layer developed naturally. Trips were not used.

Data Acquisition

Most of the data were taken in blocks of 200 records per channel (1024 data points per record) at $f_s = 200$ kHz per channel. The sampling rate selected was a compromise between the need for accurate time resolution of the shock passages (requiring high f_s) and the need to obtain a large enough number of shock passages for accurate statistics (i.e., requiring a long time span). At these high rates, the a/d converter writes directly to CPU memory so the number of records was limited to a total of 400 (200 per channel). During the test program a second a/d converter became available, and several tests were made at $f_s = 500$ kHz per channel. In the earlier test series on the flat plate, 200 records of data were acquired at $f_s = 250$ kHz per channel. Some additional tests were also performed on a single channel so that 400 records of data could be taken at the same f_s.

III. Analysis Techniques

Analysis was performed on the raw pressure signals and on the conditionally sampled signals. Some pertinent comments on the techniques used are given briefly below.

Power Spectra

Power spectral density estimates $G(f)$, in units of psi^2/Hz, were determined using a Fast Fourier Transform (FFT) based time series analysis code. The spectra were calculated using 200–400 records. The results, other than those of the undisturbed boundary layer, are plotted in the form $G(f)\cdot f/\sigma^2_{P_w}$ on linear-log axes. In this form, the area under a given curve segment is linearly proportional to the contribution of that particular frequency range to the overall signal variance $\sigma^2_{P_w}$. This makes it easier to recognize dominant frequency ranges. Normalizing by $\sigma^2_{P_w}$ forces the area to unity, which is useful for comparative purposes. However, caution is needed since this can be misleading unless the true σ_{P_w} and true spectrum have been measured. If there is a frequency cutoff, then as the area is forced to unity, the low-frequency range of the spectrum will be incorrect, even if the original dimensional spectrum is correct. For this reason, only spectra in the intermittent region are presented in normalized form.

Conditional Sampling

The pressure signal in the intermittent region (Fig. 3) consists of three components: 1) high-frequency, low-amplitude fluctuations of the incoming boundary layer; 2) high-frequency, larger-amplitude fluctuations of the flow downstream of the shock; and 3) low-frequency, high-amplitude fluctuations caused by the motion of the shock. To examine the shock motion alone, components 1 and 2 must be eliminated from the signal. This is the purpose of the conditional sampling algorithm that converts the raw pressure signals in the intermittent region into a "boxcar" as shown in Fig. 3. The boxcar has a value of unity when the algorithm determines that the shock is upstream of the transducer and a value of zero when it is downstream. In a comparative study of conditional sampling algorithms, Dolling and Brusniak[16] concluded that two-threshold methods were best for separating the pressure fluctuations caused by the shock motion from those of the boundary layer. Single threshold methods are unable to make this distinction consistently and inadvertently count high-frequency turbulent fluctuations as shock passages. The shock zero crossing frequency f_c given by

$$f_c = \frac{1}{T_m} = \frac{1}{(1/N)\sum_{i=1}^{N} T_i}$$

where T_i is the ith shock period (Fig. 3) and N the number of periods, is then unrealistically high, regardless of the selection of the threshold T. The two-threshold method is not foolproof, but is able to bracket f_c in a relatively narrow range.

The thresholds used in Ref. 11 were $T_1 = \bar{P}_{w0}$ and $T_2 = \bar{P}_{w0} + 4.5\sigma_{P_{w0}}$, where $\bar{P}_{w0}$ and σ_{Pw0} are the mean pressure and standard deviation of the incoming turbulent boundary layer fluctuations, respectively. A boxcar is generated when $P_w(t)$ rises above T_2 and is terminated when the pressure signal $P_w(t)$ falls below T_1. A problem with this approach is the requirement that $P_w(t)$ fall below $\bar{P}_{w0}$ to end a boxcar, since $P_w(t)$ does not always fall below the mean value, especially between closely spaced shock passages. Dolling and Brusniak performed a sensitivity analysis using values of $T_1 = \bar{P}_{w0} + n\sigma_{P_{w0}}$ $(0 \le n \le 3)$ and $T_2 = \bar{P}_{w0} + m\sigma_{P_{w0}}$ $(3 \le m \le 9)$ and determined that settings of $T_1 = \bar{P}_{w0} + 3\sigma_{P_{w0}}$ and $T_2 = \bar{P}_{w0} + 6\sigma_{P_{w0}}$ provided thresholds above which there was little change in f_c. In the current study, these threshold settings were used.

IV. Results

Incoming Turbulent Boundary Layers

Both boundary layers were surveyed using a pitot probe with a flattened tip of height 0.38 mm. Details of the instrumentation and calibration procedures are given by Smith.[15] Mean velocity profiles deduced assuming $T_0(y) = T_{0\infty}$ and $P(y) = P_\infty$ are shown in wall coordinates u^+ vs y^+ in Fig. 4. The properties of the two layers are given in Table 1. The velocity and integral thicknesses of the tunnel floor layer are about three times those on the plate. The plate layer develops in essentially zero streamwise pressure gradient and, consequently, the wake strength parameter Π is within the accepted range for equilibrium turbulent boundary layers. In contrast, Π for the floor layer is low. This is because the test station is close to the nozzle exit plane and the boundary layer has not recovered from the strong expansion through the nozzle. The skin friction coefficients in Table 1 were deduced from the u^+ vs y^+ fitting routine and agree well with values predicted by the van Driest II theory using M_∞ and Re_θ as inputs and assuming an adiabatic wall.

In a recent survey of fluctuating wall pressure measurements under zero pressure gradient supersonic turbulent boundary layers, Dolling and Dussauge[1] concluded that because of spatial resolution limitations there are few, if any, reliable measurements. They provide a rough, but simple criterion, based on Corcos'[17] theory for calculating the damping due to spatial integration that the transducer diameter d be such that $d < 0.04\delta$. A second criterion developed by Emmerling[18] and Schewe[19] assumes that the fluctuations are mainly influenced by the wall region. From measurements and

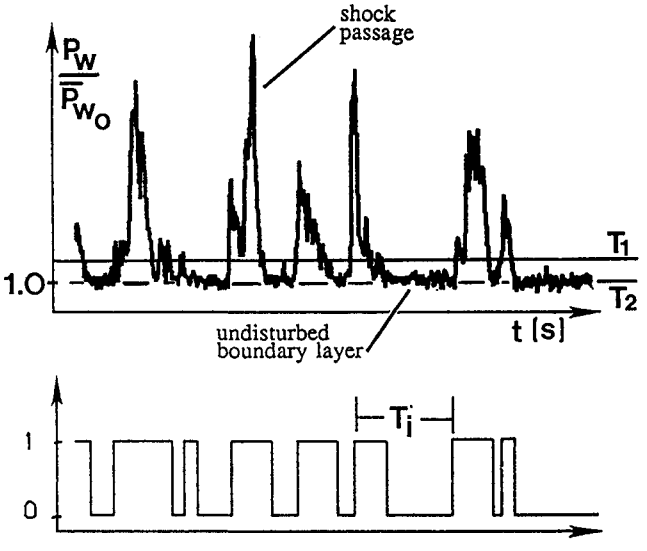

Fig. 3 Conversion of pressure signal into "boxcar."

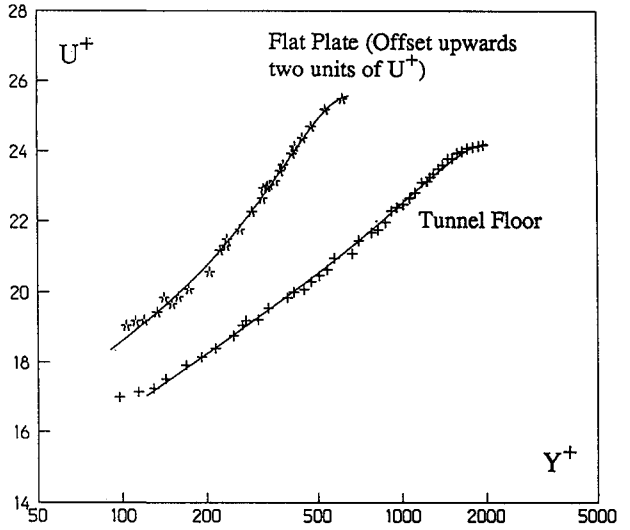

Fig. 4 Incoming mean velocity profiles in wall coordinates u^+ vs y^+.

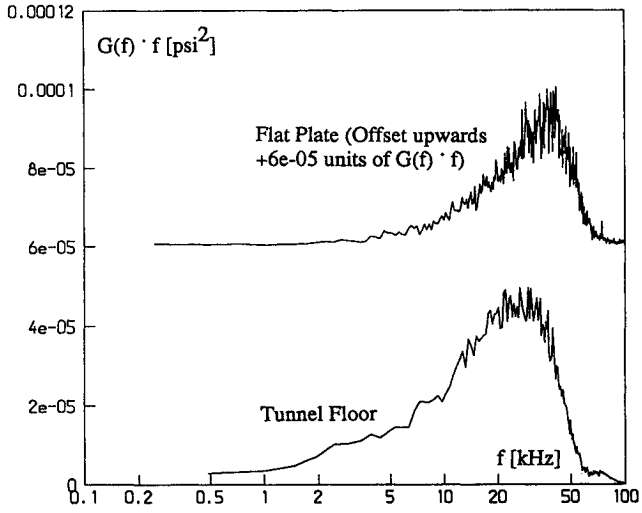

Fig. 5 Power spectral density of incoming boundary layers.

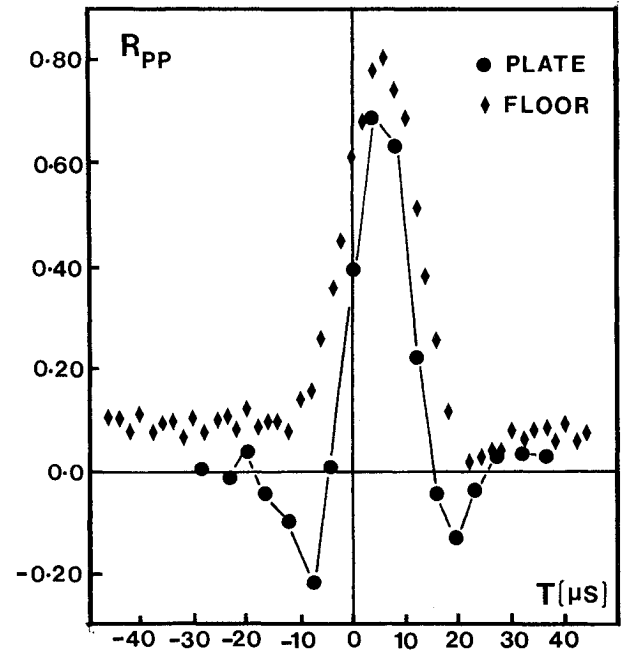

Fig. 6 Cross-correlations in incoming boundary layers.

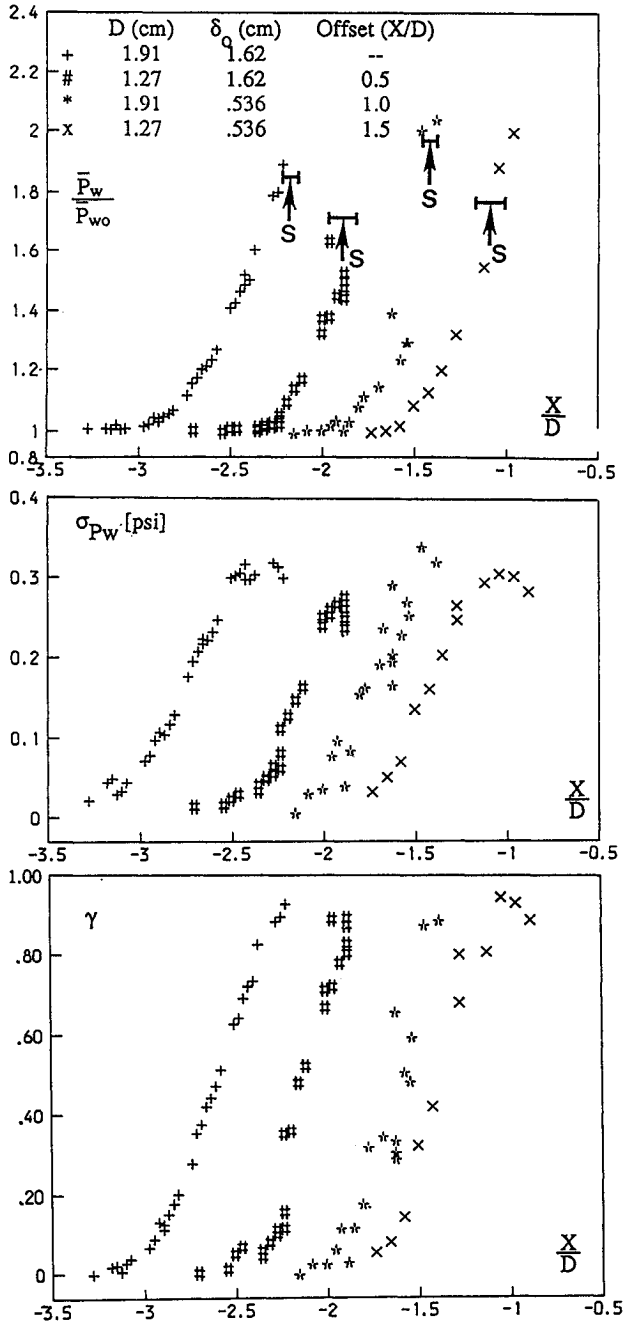

Fig. 7 Distributions of mean wall pressures, standard deviation, and intermittency.

correlations in subsonic flows, Schewe deduced that an ideal transducer should have $d < 20\nu_w/u_\tau$ where ν_w is the kinematic viscosity evaluated at the wall temperature and μ_τ the friction velocity. Schewe found an appreciable amount of energy at the "viscous" frequency u_τ^2/ν_w, even in a relatively low Reynolds number boundary layer. Dolling and Dussauge estimated that this viscous frequency is an order of magnitude below the maximum frequencies that can be found in the region of maximum production. Assuming that these results also hold in supersonic flow, two criteria for the transducer diameter and bandwidth f_b of the measuring system are $d < 20\nu_w/u_\tau$ and $f_b > u_\tau^2/\nu_w$.

Comparing this with the earlier result, $d \leq 0.04\delta$, it can be seen that both criteria cannot be met if $\delta^+ (\equiv \delta u_\tau/\nu_w) > 500$ (i.e., in high Reynolds number boundary layers). For the plate and floor boundary layers, δ^+ was about 680 and 1720, respectively. Using the smallest commercially available transducers, values of d/δ were about 0.25 and 0.1 for the plate and floor layers, respectively. The corresponding values of d^+ were about 162 and 155, a factor of about 7 greater than the "ideal" transducer. If subsonic results are even approximately applicable in supersonic flow, then the measured values of σ_{Pw} (55 and 76 N/m^{-2} for the plate and floor layers, respectively) are probably underestimated by about 40%. That the higher-frequency components of the signal are not captured is evident in the power spectral density estimates shown in Fig. 5.

Cross correlations for a streamwise spacing ξ of 2.92 mm are shown in Fig. 6. For the plate layer, $f_s = 250$ kHz is too low to resolve $(R_{pp})_{\max}$ and the delay time τ accurately. Even at twice this sampling rate, as used in the floor tests, adequate resolution is still lacking. Linear interpolations give $(R_{pp})_{\max} = 0.82$ at $\tau = 5.9$ μs and 0.84 at $\tau = 5.0$ μs for the plate and floor cases, respectively. Broadband convection velocities U_c calculated from ξ and τ at $(R_{pp})_{\max}$ were 0.72 and 0.67 U_∞ for the plate and floor layers, respectively. These values of $(R_{pp})_{\max}$ and U_c compare favorably with results from other studies.[20]

In summary, although spatial resolution and bandwidth limitations make it impossible to resolve the higher frequencies in the signal, there is no evidence of any unusual features

or properties of the fluctuating pressure field of the incoming boundary layers. Since the major focus is on the separation shock motion, which is a relatively low-frequency phenomenon, these limitations should have little impact on the accuracy of that work.

Intermittent Region

Distributions of the normalized mean wall pressure $\bar{P}_w$, the standard deviation, σ_{P_w}, and intermittency γ as functions of X/D are shown in Fig. 7. For clarity, three of the curves have been offset streamwise as indicated in the legend. The separation location, deduced from surface tracer techniques, is indicated by S (the horizontal bar indicates the effect of a $\pm$ 1 mm error in locating S).

The following point should be noted regarding $\bar{P}_w$. Because of small shifts in the transducer zero it is difficult to make accurate mean measurements at the low pressure levels (4×10^3 N m^{-2}, 0.6 psi) of this test facility. To correct for small zero shifts the following procedure was adopted. It uses the fact that the undisturbed component of the signal in the intermittent zone is that of the incoming boundary layer and has a mean value equal to the freestream static pressure P_∞. Hence, the measured mean value of this portion of the signal $\bar{P}_{\infty m}$ was set equal to P_∞. Thus, the values of $\bar{P}_w/P_\infty$ shown in Fig. 7 are actually $(\bar{P}_m - \bar{P}_{\infty m})/\bar{P}_\infty$, where $\bar{P}_m$ is the measured mean value of the entire signal. In doing this, the assumption is being made that the small dc offsets from test to test simply shift the calibration curve up or down; the transducer sensitivity does not change. Repeated calibrations show that this was indeed the case. Of course, this process is arbitrary, and the resulting mean values must be treated with caution. However, the distributions obtained exhibit the usual features seen in such interactions. Upstream influence is typical and the pressure rises rapidly to the separation point S over a streamwise distance that scales with D and not δ_0.

There is also scatter due to the difficulty of positioning the transducer. The initial mean pressure rise is steep so small that inaccuracies in position can lead to significant differences in $\bar{P}_w$. Scatter due to positioning problems is most evident in the distribution of σ_{P_w}. However, in this case, since σ_{P_w} is calculated about the mean value, small dc offsets from test to test do not contribute any error. The same comment applies to the calculation of γ.

Near the interaction start σ_{P_w} increases rapidly, reaching a maximum close to separation as observed in earlier work using blunt fins. The maximum values of about 1.7–2.07 $\times 10^3$ N m^{-2} (0.25–0.3 psia) are a significant fraction of the local mean value and, as shown in Table 2, are comparable to those measured upstream of hemicylindrically blunted fins and compression ramps at Mach 3.

From the distributions of γ shown in Fig. 7, the length scale of the shock motion Ls can be deduced. If it is defined as the distance over which γ increases from 0.05 to 0.95, then Ls is in the range 0.6–0.8 D. These values are comparable to those for the four Mach 3 fin flows cited in Table 2 that ranged from about 0.5–0.6 D.

Table 2 Maximum σ_{P_w} in intermittent region

Model/flow conditions	$(\sigma_{P_w}/\bar{P}_w)_{max}$	Ref.
Circular cylinders, $M_\infty = 5$		
D = 1.27, 1.91 cm,	0.25–0.28	—
δ = 1.62, 0.54 cm		
Blunt fins ($M_\infty = 3$)		
D = 1.27 cm, δ = 1.6 cm	0.18	2
D = 2.54 cm, δ = 1.6 cm	0.23	
D = 1.27 cm, δ = 0.4 cm	0.23	
D = 2.54 cm, δ = 0.4 cm	0.29	
Compression ramps, $M_\infty = 3$		
α = 24 deg, δ = 2.2 cm	0.2	4–6
α = 24 deg, δ = 1.2 cm	0.18	
α = 20 deg, δ = 2.2 cm	0.15	

Figure 8 shows the evolution of the normalized power spectrum through the intermittent region and at one station 0.15 D downstream of S for the 1.91 cm cylinder on the tunnel floor. The large-amplitude fluctuations generated by shock motion are broadband but centered at a low frequency, around 1 kHz. In this form, it can be seen that the larger fraction of the overall signal variance comes from the low-frequency shock oscillation. With increasing γ, the flow downstream of the shock is a larger fraction of the signal. Although the normalized curves collapse above 10 kHz, there are actually progressively higher absolute power levels at the higher frequencies since σ_{P_w} increases with increasing γ (Fig. 7). Downstream of S, the spectrum changes shape. The transducer is under the separated shear layer and the larger fraction of the signal variance is generated by the high-frequency shear layer eddies moving downstream. Consequently, in the range 10–50 kHz, the spectrum shows the same basic features as seen in the undisturbed turbulent boundary layer. A similar evolution of the power spectrum is seen in the other three test cases.

The cross correlation for transducers positioned 0.2 and 0.35 D downstream of S is shown in Fig. 9. There are two maxima in the correlation coefficient; one at $\tau \approx -18$ μs and the other at $\tau \approx +8$ μs. The latter is generated by the downstream-moving eddies in the shear layer, hence the positive τ. The broadband convection velocity, U_c is 365 m/s. For a separation shock with a pressure ratio of about 2, the velocity external to the shear layer downstream of the shock U_e would be about 0.97 U_∞ ($\approx$ 718 m/s); hence, $U_c/U_e \approx 0.51$. This is a lower ratio than in the incoming boundary layer, but since the velocity profile close to S is more retarded, a lower convection velocity would be anticipated.

The maximum at negative τ corresponds to an upstream velocity of 162 m/s and is probably generated by the reverse flow. In this case, 162 m/s is 0.22 U_∞, which compares favorably with measurements made by Ozcan and Holt[21] upstream of circular cylinders at Mach 2.36. Using laser anemometry, maximum reverse flow velocities of 0.2 U_∞ were measured. That reverse flow velocities of this magnitude would be expected is evident in the numerical simulations of Hung and Buning[22] (for a Mach 3 hemicylindrically blunted fin) and the measurements of Voitenko et al.[23] using cylinders at Mach 2.5. Both simulation and experiment show an embedded region of supersonic reverse flow. In the present experiment,

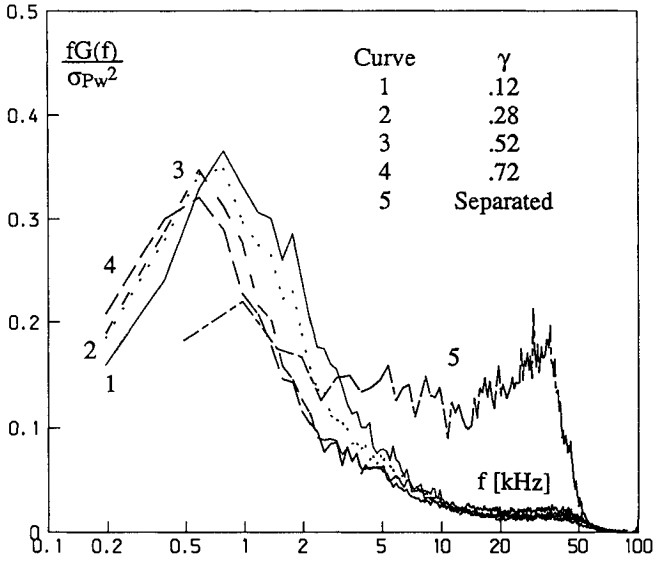

Fig. 8 Evolution of normalized power spectrum through intermittent region (D = 1.91 cm, tunnel floor).

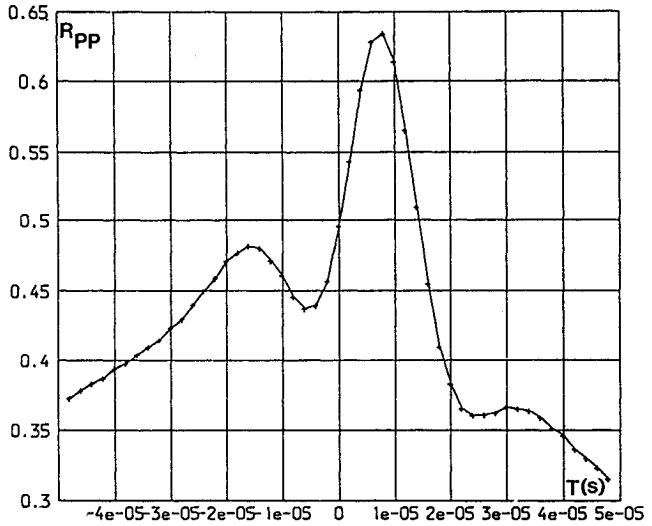

Fig. 9 Cross correlation of pressure signals downstream of S ($D = 1.91$ cm, tunnel floor).

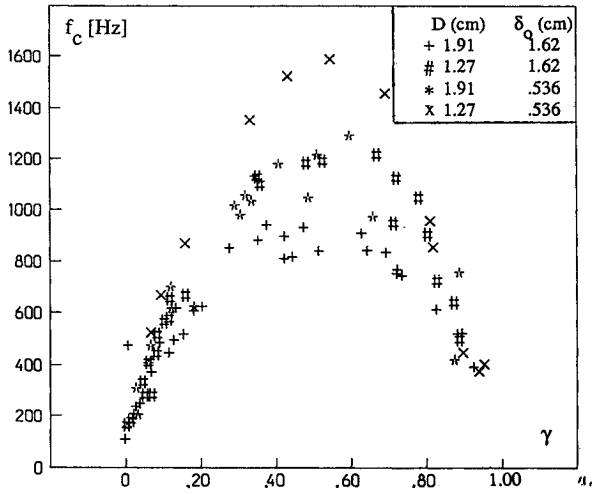

Fig. 11 Shock zero-crossing frequency as a function of intermittency (all test cases).

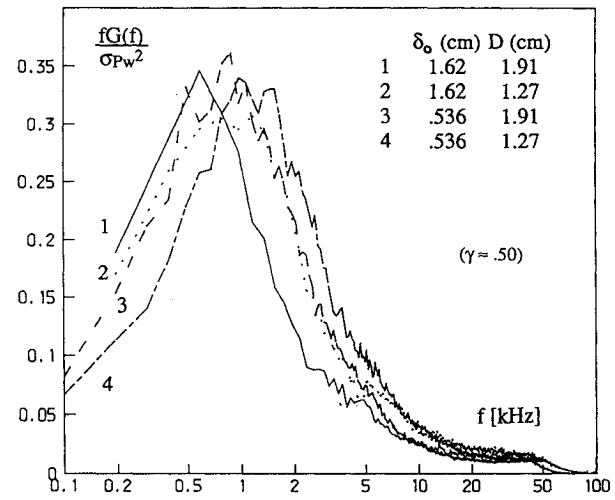

Fig. 10 Power spectra at $\gamma \approx 0.5$ (all test cases).

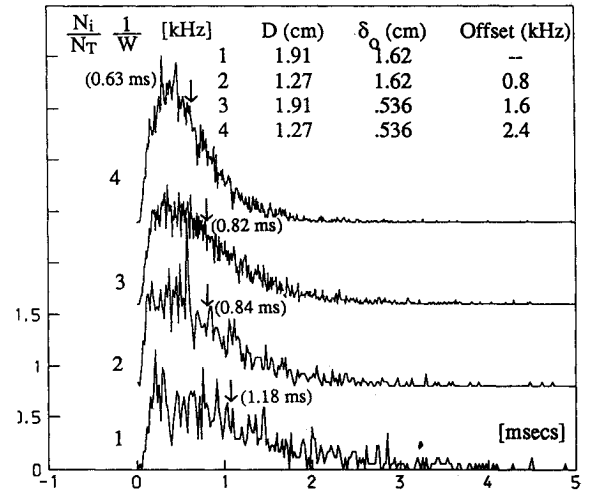

Fig. 12 Probability density distributions of shock periods at $\gamma \approx 0.5$ (all test cases).

the transducers are upstream of where this embedded region would be expected, but even near S the simulations indicate reverse flow Mach numbers of about 0.4. Assuming the static temperature is close to the wall value, 162 m/s corresponds to a Mach number of 0.4–0.5, which is in good agreement with this.

Power spectra at $\gamma \approx 0.5$ for all four test cases are shown in normalized form in Fig. 10. Their shapes and maximum power levels are essentially the same. Although resolution at low frequency is not adequate to resolve all the details, there is clearly a shift in the center frequency from case to case. For fixed δ, an increase in D decreases the center frequency. For fixed D, the center frequency is lower in the thicker boundary layer. In all four cases, the center frequency is one to two orders of magnitude less than the large eddy frequency U_e/δ of the incoming boundary layer. Power spectra at other values of γ show the same trends. These observations are supported by the distributions of zero-crossing frequency f_c shown in Fig. 11. These were calculated using the conditional sampling algorithm described earlier. The maximum values occur at $\gamma \approx 0.5$ and, as the power spectra indicated, are low, and $(f_c)_{\max}$ exhibits the same trends with D and δ_0 as the spectral center frequencies.

The probability density distributions of the shock wave periods T_i are shown in Fig. 12. The vertical axis is given by $(N_i/N_T) \times (1/W)$, where N_i is the number of periods within a given interval, N_T the total number of periods counted, and W the width of the interval in seconds. For the flat-plate test cases, $W = 4$ μs; for the tunnel floor cases, $W = 20$ μs. The mean period T_m, which is the inverse of f_c, is indicated by the vertical arrow on each curve. The shapes of the distributions and general trends are the same in all four cases. For a fixed D, the maximum shock period is higher in the thicker boundary layer and the probability of finding shorter periods is lower. In a given boundary layer, these same trends are observed with increasing D. Although the data have some scatter, particularly for the tunnel floor cases for which fewer records were taken, there is little evidence of any significant change in the magnitude of the most probable period T_p, from one test case to another. Although it cannot be pinpointed precisely, T_p is in the range 0.2–0.5 ms.

The corresponding probability density distributions for the shock frequency f_i are shown in Fig. 13. Since $f_i = 1/T_i$, the distributions of f_i and T_i are not linearly related, so the inverse of the mean period is not the mean frequency $\bar{f}$. The latter is given by

$$\bar{f} = \frac{1}{N}\sum_{i=1}^{N} f_i = \frac{1}{N}\sum_{i=1}^{N}\frac{1}{T_i}$$

The distributions are also plotted as $(N_i/N_T) \times (1/W)$, but in this case, the interval $W(\equiv f_i - f_{i+1})$ is not constant. It

decreases as T_i increases. The curves, particularly those for the tunnel floor tests, exhibit considerable scatter for the same reasons given above. The mean frequencies $\bar{f}$ are indicated by the vertical arrows. Although the range of possible shock frequencies is broad, low frequencies (typically $<1-2$ kHz) are most probable in all cases. For a fixed D, the mean and most probable frequencies decrease in the thicker boundary layer.

From the boxcar representation of the pressure signals of pairs of transducers placed streamwise in the intermittent region, the time delay T_r between the shock crossing the downstream transducer and then the upstream one can be deduced (see inset to Fig. 14). Similarly, as the shock moves downstream, the delay time T_d can be deduced. From these times and the transducer spacing, the shock speeds in both directions can be calculated. An example showing the distribution of shock speeds in both directions for the 1.91 cm cylinder in the floor boundary layer is shown in Fig. 14; U_s is the shock speed, N the number of occurrences of a given speed, and N_T the total number of events (typically 400–700, depending on the test case and intermittency). For this case, $\gamma = 0.45$ for the upstream transducer and 0.65 for the downstream one. Mean upstream and downstream speeds are very low, typically 0.06–0.07 U_∞, and are independent of position in the intermittent region and incoming boundary-layer properties, but weakly dependent on the cylinder diameter. Downstream values are typically 10% higher than upstream values. Andreopoulos and Muck[5] have made similar calculations in a Mach 3 separated compression ramp flow. The small number of nested wave pairs (only 65) precluded an accurate result but gave speeds in the range of 0.05–0.8 U_∞, with a mean value of about 0.15 U_∞. Upstream and downstream values were about the same. It is quite probable that different mean values occur in different flows, but it is also possible that the higher mean in the compression ramp flow could be due to use of a single threshold algorithm to generate the boxcars. This biases the results to shorter times and hence higher speeds.

V. Discussion

Analysis of the separation shock dynamics for the four test cases shows that both D and δ influence the motion. The mean and zero-crossing frequencies are low compared to the typical large eddy frequency in the boundary layer and, although the range of shock frequencies extends up to about 10 kHz, frequencies less than about 2 kHz are much more probable. Shock speeds are also very low, with mean values a small fraction of U_∞, and are about the same in both upstream and downstream directions. There is some evidence that the latter are slightly higher. Bearing in mind that the two incoming boundary layers have very different histories and that typical large eddy frequencies differ by a factor of about 3 : 1, the effect of changes in the incoming flow are relatively small. These observations prompt the obvious question of what mechanism is responsible for these results.

It has been suggested by Andreopoulos and Muck[5] that "turbulence of the incoming boundary layer is largely responsible for the shock wave motion." This conclusion stemmed from the observations that the zero-crossing frequency was the same order as the estimated bursting frequency in the incoming boundary layer and that shock velocities were of the same order as velocity fluctuations in the flowfield. The present authors consider this direct linkage with turbulent

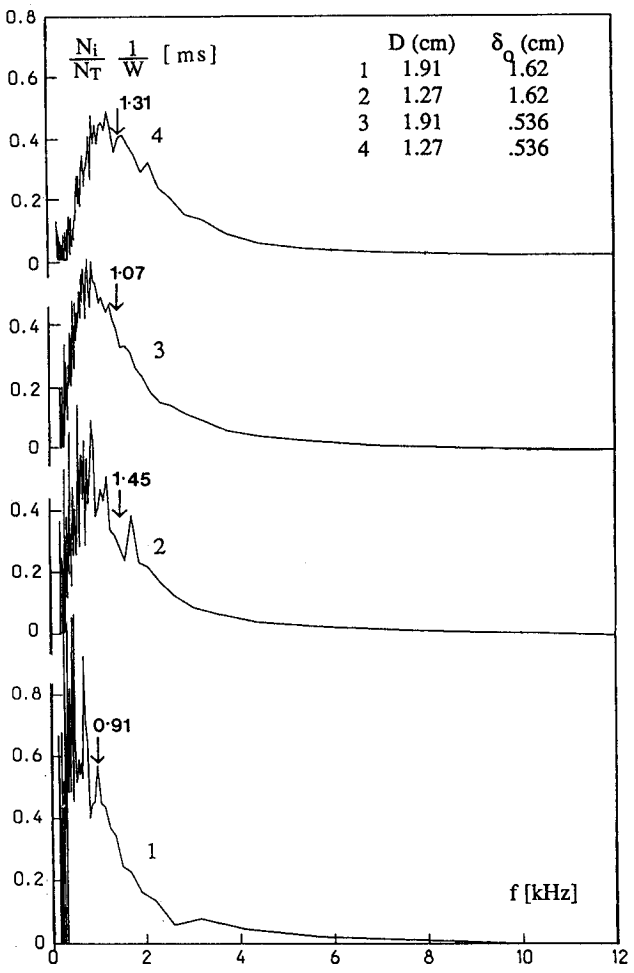

Fig. 13 Probability density distributions of shock frequencies at $\gamma \approx 0.5$ (all test cases).

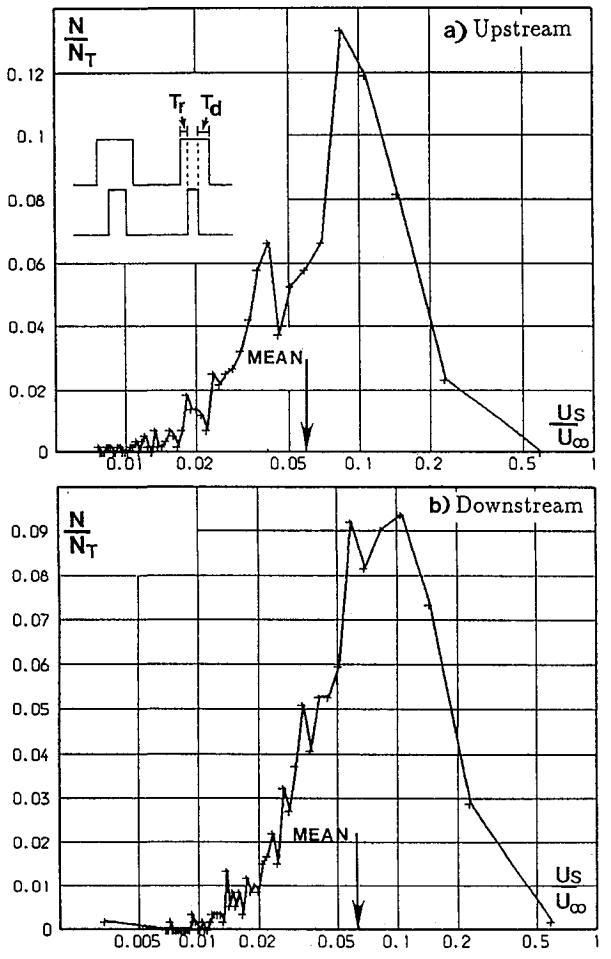

Fig. 14 Probability density distributions of shock speeds in upstream and downstream directions ($D = 1.91$ cm, tunnel floor).

fluctuations in the incoming boundary layer somewhat speculative for several reasons: 1) the bursting frequency was not measured; 2) the shock frequency was obtained using a single threshold conditional sampling algorithm and, as shown in Ref. 16, this can lead to unrealistically high frequencies; and 3) it is not necessary that the shock motion be connected with transport phenomena—the shock is an interface and its propagation speed depends on the instantaneous pressures P_1 and P_2 in the upstream and downstream regions, respectively. A simple model, based on the latter idea, is developed below.

Relative to the separated flow downstream of the shock wave, the upstream flow (i.e., incoming undisturbed turbulent boundary layer) has pressure fluctuations that are one order of magnitude or more lower. If the latter are considered negligible, then conditions upstream may be considered constant and the shock propagation speed is affected only by the larger downstream fluctuations. The instantaneous shock velocity W in the streamwise direction can be written as

$$W = \frac{a_1}{\sin\beta}\left[\frac{\gamma+1}{2\gamma}\left(\frac{P_2}{P_1}-1\right)+1\right]^{\frac{1}{2}}$$

where a_1 is the speed of sound in the upstream region, β the shock angle, and γ the ratio of specific heats. The measured separation pressure ratio is about 1.9, which for an incoming Mach number of 4.9 corresponds to a shock angle of about 15.7 deg. These values give $W = 740$ m/s, the freestream velocity. In this simple model with a_1, β, γ, and P_1 fixed, W will depend only on changes in P_2. Measurements at the upstream edge of the separated flow show that σ_{P_W} is about 1400 N m^{-2} (0.2 psi) and the amplitude probability density distribution is Gaussian. Hence, P_2 varies approximately ± 4200 N m^{-2} (± 0.6 psi) about its mean value of 1.9 P_∞ with smaller amplitudes more probable. Table 3 below shows the changes in W/U_∞ from the equilibrium value of unity that are obtained by varying P_2 by $\pm n\sigma_{P_W}$, where $1 \le n \le 3$. Positive increments in P_2 increase W (i.e., upstream excursion of shock) and vice-versa.

Comparison of the tabulated results with the measured shock speeds suggests a correlation. First, except in the first case (due to the nonlinearity of the equation), the calculated downstream speed is about 10–20% higher than the upstream value, a feature observed experimentally. Second, since the amplitude distribution of the pressure fluctuations is essentially Gaussian, a larger fraction of the fluctuations will have smaller amplitudes than larger amplitudes. This would bias the shock speeds to small fractions of U_∞, also a feature seen experimentally. Third, the predicted maximum speeds, which would correspond to fluctuations with amplitudes of $\pm 3\sigma_{P_W}$, correlate well with the measured ones. The very small fraction of shock speeds found at 0.5 U_∞ in Fig. 14 could well be a result of the conditional sampling algorithm. Although the two-threshold technique discriminates between shock-induced and turbulent fluctuations better than one-threshold techniques there are occasions when it fails which would produce high calculated shock speeds.

At this stage this model must be viewed with caution. However, since it reproduces several of the observed experimental features it probably warrants further investigation. This requires an experiment using several pressure transducers in which pressure fluctuations at the upstream edge of the separated flow are correlated with shock direction and speed.

Table 3 Estimated shock speeds

	$\Delta W/U_\infty$	
Pressure change	Upstream	Downstream
$P_2 \pm 1\sigma_{P_W}$	0.072	0.065
$P_2 \pm 2\sigma_{P_W}$	0.140	0.166
$P_2 \pm 3\sigma_{P_W}$	0.206	≈ 0.249

VI. Concluding Remarks

Wall pressure fluctuations have been measured under the unsteady separation shock in interactions induced by unswept circular cylinders. Models were tested in the turbulent boundary layers on the tunnel floor ($\delta_0 = 1.62$ cm) and on a full-span flat plate ($\delta_0 = 0.54$ cm). The nominal freestream Mach number was 5, the freestream unit Reynolds number 53×10^6 m^{-1}, and the wall temperature close to the adiabatic value. Conditional sampling algorithms were used to analyze the pressure signals measured under the unsteady separation shock wave. The results show the following:

1) Shock zero-crossing frequency varies with the cylinder diameter and incoming boundary layer thickness. In a fixed boundary layer, it decreases with increasing cylinder diameter and for a fixed-diameter cylinder it is lower in a thicker boundary layer. In all cases, the zero-crossing frequency is low (typically of order 1 kHz) and is a very small fraction of the incoming boundary-layer, large-eddy frequency.

2) Probability density distributions of the shock frequencies show that although maximum values of up to 10 kHz occur, low values in the range 1–2 kHz are the most probable.

3) Probability density distributions of shock speeds in the upstream and downstream directions show that the maximum values are about 20% of the freestream velocity, while the mean value is about 6% of the freestream velocity. Mean shock speeds are independent of the position in the intermittent region and incoming boundary-layer properties but weakly dependent on cylinder diameter. Downstream values are typically 10% higher than upstream values.

4) A simple analytic model that predicts the shock speeds and their trends reasonably well suggests that the shock motion may be driven by low-frequency pressure fluctuations under the separated shear layer. This is an inferred result and remains to be proved through direct measurement.

Acknowledgments

A large fraction of the work reported in this paper was sponsored by Air Force Office of Scientific Research (AFOSR) Grant 86-0112 (monitored by Drs. J. Wilson and L. Sakell) and by the Center of Excellence of Hypersonics Training and Research (supported by NASA, AFOSR, and Office of Naval Research) at the University of Texas at Austin. These sources of support are gratefully acknowledged.

References

[1]Dolling, D. S. and Dussauge, J. P., "Fluctuating Wall Pressure Measurements," "A Survey of Measurements and Measuring Techniques in Rapidly Distorted Compressible Turbulent Boundary Layers," AGARDograph 315, Nov. 1988, Chap. 8.

[2]Dolling, D. S. and Bogdonoff, S. M., "An Experimental Investigation of the Unsteady Behavior of Blunt Fin-Induced Shock Wave Turbulent Boundary Layer Interactions," AIAA Paper 81-1287, June 1981.

[3]Dolling, D. S. and Murphy, M. T., "Unsteadiness of the Separation Shock Wave Structure in a Supersonic Compression Ramp Flowfield," *AIAA Journal*, Vol. 21, Dec. 1983, pp. 1628-1634.

[4]Dolling, D. S. and Or, C. T., "Unsteadiness of the Shock Wave Structure in Attached and Separated Compression Ramp Flowfields," *Experiments in Fluids*, Vol. 3, 1985, pp. 24-32.

[5]Andreopoulos, J. and Muck, K. C., "Some New Aspects of the Shock Wave Boundary Layer Interaction in Compression Ramp Flows," *Journal of Fluid Mechanics*, Vol. 180, 1987, pp. 405-428.

[6]Dussauge, J. P., Muck, K. C., and Andreopoulos, J., "Properties of Wall Pressure Fluctuations in Separated Flow Over a Compression Ramp," *Proceedings, IUTAM Symposium, Turbulent Shear-Layer/Shock-Wave Interactions*, Springer-Verlag, Berlin, 1985.

[7]Tan, D. K. M., Tran, T. T., and Bogdonoff, S. M., "Surface Pressure Fluctuations in a Three Dimensional Shock Wave/Turbulent Boundary Layer Interaction," AIAA Paper 85-0125, Jan. 1985.

[8]Tran, T. T., Tan, D. K. M., and Bogdonoff, S. M., "Surface Pressure Fluctuations in a Three Dimensional Shock Wave/Turbulent Boundary Layer Interaction at Various Shock Strengths," AIAA Paper 85-1562, July 1985.

[9]Tran, T. T., "An Experimental Investigation of Unsteadiness in Swept Shock Wave/Turbulent Boundary Layer Interactions," Ph.D. Dissertation (T-1763), Mechanical and Aerospace Engineering Dept., Princeton Univ., Princeton, NJ, 1987.

[10]Dolling, D. S. and Narlo, J. C., II, "Driving Mechanism of Unsteady Separation Shock Motion in Hypersonic Interactive Flow," *Aerodynamics of Hypersonic Lifting Vehicles*, AGARD-CP-428, Nov. 1987.

[11]Narlo, J. C., II, "Experimental Investigation of the Driving Mechanisms of Separation Shock Wave Motion in Interactive Flows," MS Thesis, Aerospece Engineering and Engineering Mechanics Dept., Univ. of Texas at Austin, Austin, TX, 1986.

[12]Hanly, R. D., "Effects of Transducer Flushness on Fluctuating Surface Pressure Measurements," AIAA Paper 75-534, March 1975.

[13]Dolling, D. S. and Bogdonoff, S. M., "Scaling of Interactions of Cylinders with Supersonic Turbulent Boundary Layers," *AIAA Journal*, Vol. 19, May 1981, pp. 655-657.

[14]Raman, K. R., "Surface Pressure Fluctuations in Hypersonic Turbulent Boundary Layers," NASA CR 2386, Feb. 1974.

[15]Smith, D. R., "The Effects of Incoming Boundary Layer Thickness on Unsteady Shock-Induced Turbulent Separation Induced by Cylinders, MS Thesis, Dept. of Aerospace Engineering and Engineering Mechanics, University of Texas at Austin, Austin, TX, Dec. 1987.

[16]Dolling, D. S. and Brusniak, L., "Separation Shock Motion in Fin, Cylinder and Compression Ramp-Induced Turbulent Interactions," AIAA Paper 87-1368, June 1987.

[17]Corcos, G. M., "Resolution of Pressure in Turbulence," *Journal of the Acoustical Society of America*, Vol. 35, No. 2, 1963, pp. 192-199.

[18]Emmerling, R., "The Instantaneous Structure of the Wall Pressure Under a Turbulent Boundary-Layer Flow," Max-Planck Institut fur Stromungforschung, Rept. 9/1973, D-3400 Göttinger, West Germany.

[19]Schewe, G., "On the Structure and Resolution of Wall Pressure Fluctuations Associated with Turbulent Boundary-Layer Flow," *Journal of Fluid Mechanics*, Vol. 134, 1983, pp. 311-328.

[20]Dolling, D. S. and Smith, D. R., "Unsteady Shock-Induced Turbulent Separation in Mach 5 Cylinder Interactions," AIAA Paper 88-0305, Jan. 1988.

[21]Ozcan, O. and Holt, M., "Supersonic Separated Flow Past a Cylindrical Obstacle on a Flat Plate," *AIAA Journal*, Vol. 22, May 1984, pp. 611-617.

[22]Hung, C. M. and Buning, P. G., "Simulation of Blunt Fin-Induced Shock Wave and Turbulent Boundary Layer Interaction," AIAA Paper 84-0457, Jan. 1984.

[23]Voitenko, D. M., Zubkov, A. I., and Panov, Y. A., "Existence of Supersonic Zones in Three Dimensional Separated Flows," *Izvestiya Akademii Nauk USSR, Mekhanika Zhindkosti i Gaza*, Vol. 2, Jan.-Feb. 1967, pp. 2-24.